RSC Advances

Varying Numbers and Positions of Carboxylate Groups on Ru Dyes for Dye-Sensitized Solar Cells: Uptake to TiO2, Cell Performance and Cell Stability

Journal:	*RSC Advances*
Manuscript ID:	RA-ART-12-2013-047795.R1
Article Type:	Paper
Date Submitted by the Author:	23-Jan-2014

Complete List of Authors:	Hewat, Tracy; University of Edinburgh, McDonald, Shane; University of Bath, Department of Chemistry Lee, Jonathan; Solar Print, Rahman, Mahfujur; Solar Print, Cameron, Petra; University of Bath, Chemistry Hu, Fu-Chun; National Tsing-Hua University, Chi, Yun; National Tsing Hua University, Chemistry Yellowlees, Lesley; University of Edinburgh, Department of Chemistry Robertson, Neil; Edinburgh University, Department of Chemistry

Table of Contents Graphic:

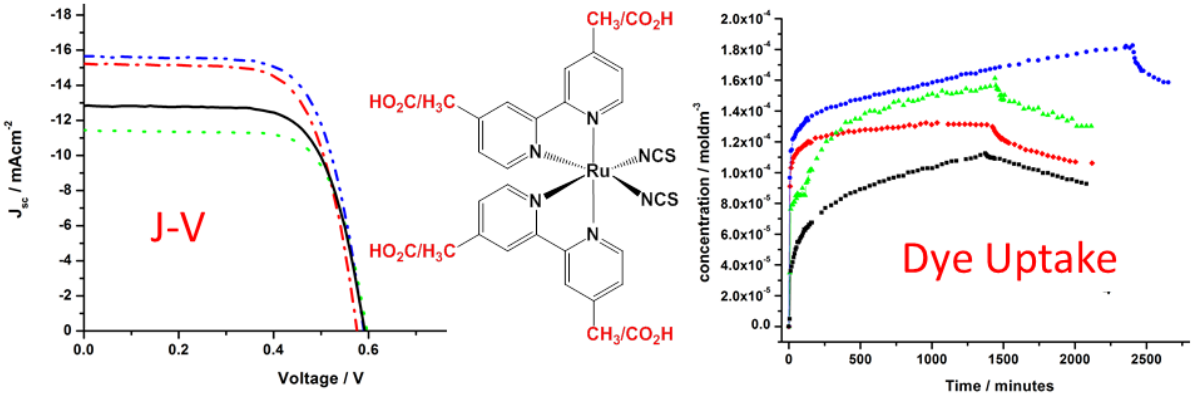

Varying the number and position of carboxylate groups on Ru(II) dyes affects the efficiency, dye uptake, dye binding and stability of dye-sensitised solar cells.

Cite this: DOI: 10.1039/c0xx00000x

www.rsc.org/MaterialsA

PAPER

Varying Numbers and Positions of Carboxylate Groups on Ru Dyes for Dye-Sensitized Solar Cells: Uptake to TiO_2, Cell Performance and Cell Stability

Tracy Hewat,[a] Shane McDonald,[b] Jonathan Lee,[c] Mahfujur Rahman,[c] Petra Cameron,*[b] Fa-Chun Hu,[d] Yun Chi,*[d] Lesley J. Yellowlees,[a] Neil Robertson*[a]

Received (in XXX, XXX) Xth XXXXXXXXX 20XX, Accepted Xth XXXXXXXXX 20XX

DOI: 10.1039/b000000x

Four simple ruthenium(II) dyes have been synthesised with the general formula [Ru(4,4'-(R,R_1)-bipyridine)(4,4'-(R_2,R_3)-bipyridine)$(NCS)_2$] where R, R_1, R_2 and R_3 represent CH_3 or CO_2H, hence varying the number and position of the carboxylic acid groups that bind the dye to TiO_2. The effect of varying the acid groups on cell fabrication, electrical performance and stability has been studied. The photophysical and electrochemical properties have been recorded and are relatively similar across the dye series, all showing parameters consistent with successful cell function, suggesting these dyes can be used as a good model to investigate the effect of changing the acid binding groups. Device measurements showed that the dyes containing a 4,4'-dicarboxy-bipyridine ligand, with two CO_2H groups on same bipy, gave higher short-circuit current than the dyes that had ligands with no more than one carboxylate group on a given bipy. Measurement of dye uptake to TiO_2 using optical waveguide spectroscopy suggested that the dye with three acid groups provided better dye coverage, faster dye uptake rate, and a greater amount of dye remaining in the cell after rinsing. All four dyes gave cells that were broadly thermally stable at 85 ^oC over 500 hours, however the dye with only one acid group showed poorer thermal stability than the others.

Introduction

Dye-sensitised solar cells (DSSC) have emerged as a leading approach to the development of low-cost, flexible and coloured photovoltaics, complementary to established technologies such as silicon.[1,2,3] Dye design remains one of the most important and challenging areas for achieving highly-efficient and stable dye-sensitized solar cells leading to extensive research into metal complex,[4,5,6] organic,[7] porphyrin,[8] and phthalocyanine[8,9] dyes. A dye must contain at least one anchoring group to bind successfully to the surface of a semiconductor whilst maintaining efficient charge injection. Most commonly, a carboxylic acid functionality is used to interact with the hydroxyl groups on the surface of TiO_2 and bind via ester linkages.[10]

The dye diffusion through the nanoporous network, uptake of the dye on the surface of titania and stability once bound depend on the number of anchoring groups present and can significantly affect the manufacturability and efficiency of the cell.[11] Cell operation is related to the energetic and kinetic processes in a solar cell that drive charge injection into TiO_2, charge recombination and dye regeneration,[12] which are all influenced by the binding mode to the oxide.

Theoretical modelling by De Angelis and co-workers[13] has explored the preferred number of binding groups for a dye to successfully anchor to the surface of TiO_2, suggesting that binding through three linkages is energetically and sterically feasible. They suggest in particular that binding through three carboxylic acid groups is a route to obtaining higher open-circuit voltage (V_{OC}). The stability of the solar cell towards dye desorption can also be improved if the dye contains three anchoring groups.[13] In addition, recent studies suggest that the number of carboxylate groups plays an important role in dipole formation at the TiO_2 surface through interactions with electrolyte additives such as Li^+ or *t*-butylpyridine. This in turn affects charge injection dynamics.[14] These observations are particularly crucial when considering that the large majority of organic sensitisers for DSSC possess only one anchoring unit, commonly cyanoacrylic acid.[7] To the best of our knowledge there have been no systematic studies to experimentally probe the effect of changing the number and position of carboxylate groups on the sensitiser dye. Accordingly, we believe that the design and development of new sensitisers would benefit from greater

systematic comparison of related dyes possessing differing numbers of binding groups.

The work reported here investigates a series of simple ruthenium(II) dyes with varying number and positions of carboxylic acid groups on the bipyridyl ligands. This series of dyes has been used to study the effect of the binding groups on the overall performance of the solar cell, including both cell fabrication and cell operation.

Results and Discussion

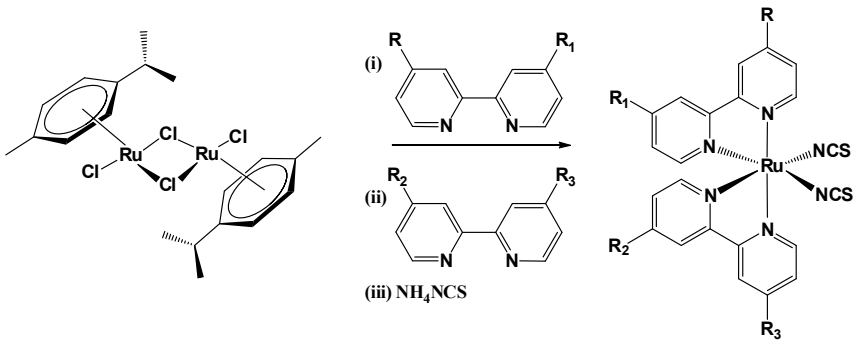

$R=R_1=CH_3$, $R_2=CH_3$, $R_3=CO_2H$ **1**

$R=R_1=CH_3$, $R_2=R_3=CO_2H$ **2**

$R=R_2=CH_3$, $R_1=R_3=CO_2H$ **3**

$R=CH_3$, $R_1=R_2=R_3=CO_2H$ **4**

Scheme 1 Synthesis of ruthenium(II) complexes reported in this work.

Syntheses

The complexes were synthesised following a standard procedure previously established for the dye Z907,[15] where the addition of the first bipyridine contains the fewer number of acidic groups, and is added at a lower temperature. Scheme 1 illustrates the steps taken to obtain the desired complexes, **1-4**.

The dyes were purified on Sephadex using DMF as the eluent and were shown to be pure by NMR and elemental analysis after only one column in a relatively good yield. One of the bipy ligands is asymmetric (4-methyl-4'-carboxy-2,2'-bipridine). When this ligand coordinates to Ru along with another bipy and two isothiocyanate groups, the resulting complex can exhibit geometric isomerism, where the methyl or carboxyl groups are *cis* or *trans* to the isothiocyanate groups (ESI†, Fig. S1, Table S1). We found however, that the isomers could not be separated through chromatography on Sephadex LH-20. Although this adds additional considerations to interpretation of the work, the effects on dye uptake, device stability, and binding to TiO_2 still gives rise to clear trends in the series regardless of the presence of isomers (*vide infra*). In the following sections, we firstly consider the properties of the dyes themselves and subsequently investigate the consequences of the structure on the fabrication, electrical properties and stability of standard dye-sensitised solar cells.

Absorption and Emission Spectroscopy

Electronic absorption spectra were recorded in DMF at varying concentrations (Fig. 1, Table 1). The first two absorption bands in the visible region represent t_{2g}-π^* transition (MLCT) and the bands in the UV region represent π-π^* transitions of the bipyridine ligands. Some changes are observed in the 350-500 nm region upon varying electron-withdrawing groups (CO_2H), however relatively small effects are seen on the position of the low-energy absorption around 540 nm.[16] All four dyes have a lower molar absorption coefficient than the N3 dye with four CO_2H groups (14200 $M^{-1}cm^{-1}$),[17] slightly reducing the light harvesting efficiency for complexes **1-4**.

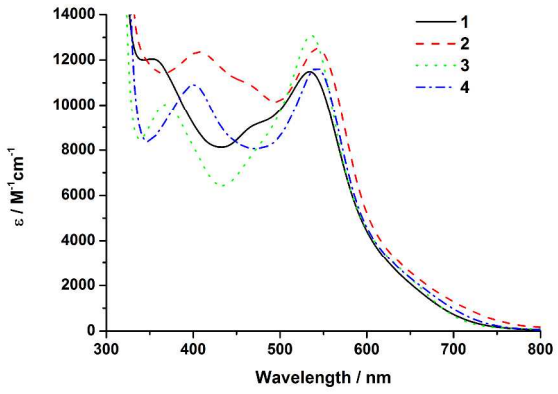

Fig. 1 Absorption spectra of **1-4** in DMF

Emission studies were carried out in degassed DMF at room temperature and 77 K. The complexes showed detectable phosphorescence only at 77 K, with room temperature emission quenched, possibly via a thermally-accessible ^{3}MC state.[18] The following analysis refers to the data collected at 77 K (Fig. 2, Table 1). All four complexes show a large spectral shift between excitation and emission maxima, suggesting ^{3}MLCT emission. The emission maximum shifts to lower energy for **2** and **4** which each contain a bipy ligand bearing two electron-withdrawing groups (CO_2H) in contrast with **1** and **3**.

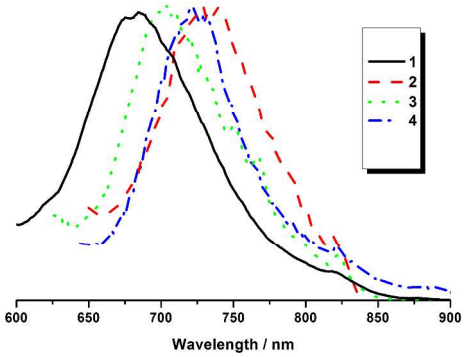

Fig. 2 Emission spectra of complexes **1-4** in DMF matrix at 77 K.

Table 1 Photophysical properties for complexes **1-4** in DMF.

Compound	λ_{abs} / nm ($\varepsilon_{max}/10^3$ M^{-1}cm^{-1})	77 K	
		Excitation λ_{max} / nm	Emission λ_{max} / nm
1	353 (12) 534 (11.5)	500	680
2	407 (12.4) 543 (12.5)	520	725
3	369 (10) 536 (13.1)	510	700
4	401 (10.9) 543 (11.7)	525	725

Electrochemistry

The electrochemical properties of complexes **1-4** are reported in Table 2 with voltammograms shown in ESI† (Fig. S4). The oxidation is assigned as the Ru(II)/Ru(III) couple with values in a range consistent with that observed for N3 (1.13 V).[15, 17] Slight shifts are observed due to the change in functionality between complexes **1-4**; with a greater number of acid groups on bipyridine the oxidation potential shifts to more positive values. The I_2^-/I^- couple, which is thought to be responsible for dye regeneration, has a potential of 0.79 V (*vs.* NHE in acetonitrile),[19] which suggests there is enough driving force to regenerate the dyes reported in this work.

The potential of the first reduction also varies according to the functionality on bipyridine. Complex **1** shows two pseudo-reversible waves which can be attributed to reduction of 4,4'-dimethyl-2,2'-bipyridine and 4-methyl-4'-carboxy-2,2'-bipyridine, the latter assumed to reduce first due to the electron-withdrawing nature of a carboxyl group. Similarly, complex **2** shows a pseudo-reversible wave representing the reduction of 4,4'-dicarboxy-2,2'-bipyridine. The second reduction wave is masked by the solvent window. Complex **4** has a slightly more negative reduction potential than expected, however in general all four complexes show similar values.

Complexes **2** and **3** differ in structure by the position of the two carboxyl groups. Complex **2** has both carboxyl groups on the same bipyridine whereas complex **3** has one carboxyl group on each bipyridine. Interestingly, there is no difference in electrochemical potentials between complex **2** and **3**, suggesting that the position of the acid groups on each bipyridine ligand does not have a strong influence on the overall ground-state electrochemical properties of the dye. The excited state reduction potential of the dyes can be readily calculated by the expression $E°*_{ox} = E_{ox} - E_{0\text{-}0}$ giving values of -1.05 (**1**), -0.85 (**2**), -0.91 (**3**) and -0.79 V (**4**). These are all significantly more negative than the conduction band of the TiO_2 (-0.50 V against NHE) hence charge injection into the TiO_2 is expected to be rapid and efficient.

Table 2 Electrochemical data for complexes **1-4** in 0.1 M $TBABF_4$/DMF *vs.* NHE.

Compound	E_{ox} / V	E_{red} / V
1	1.00 [a]	-1.28 [b] -1.59 [b]
2	1.06 [b]	-1.30 [b]
3	1.06 [b]	-1.30 [b]
4	1.11 [b]	-1.36 [b]

[a] irreversible

[b] pseudo-reversible

Computational and Electronic Properties of the dyes

Hybrid-DFT (ESI† Table S2 – S5) and TD-DFT (ESI† Table S6 – S9) calculations suggest that all four dyes show characteristics typical of related Ru(II) dyes.[20] The lowest energy transitions consist of a mixture of MLCT, LC, and LL'CT (NCS – bipy) character, leading to good separation of charge density in the excited state. TD-DFT (Fig. 3) calculations indicate that the calculated spectra for the combination of isomers correlates relatively well with the experimental values.

In summary, the absorption, electrochemical and computational data for all four complexes are largely comparable with each other, suggesting the electronic properties are not greatly affected by the change in the number of acid groups. In particular, the core requirements for a functioning dye in terms of light-harvesting, oxidation, excited-state reduction potential and charge-separated excited state are all in the range required for high-efficiency cells. We anticipate therefore that the performance of the dyes in solar cell studies will be more influenced by the number of anchoring groups (CO_2H), hence the binding to and electronic interaction with TiO_2, rather than the underlying photophysical and electrochemical properties of the free molecules. In this respect, the series represents a good model system to explore these binding factors.

Cite this: DOI: 10.1039/c0xx00000x

www.rsc.org/MaterialsA

PAPER

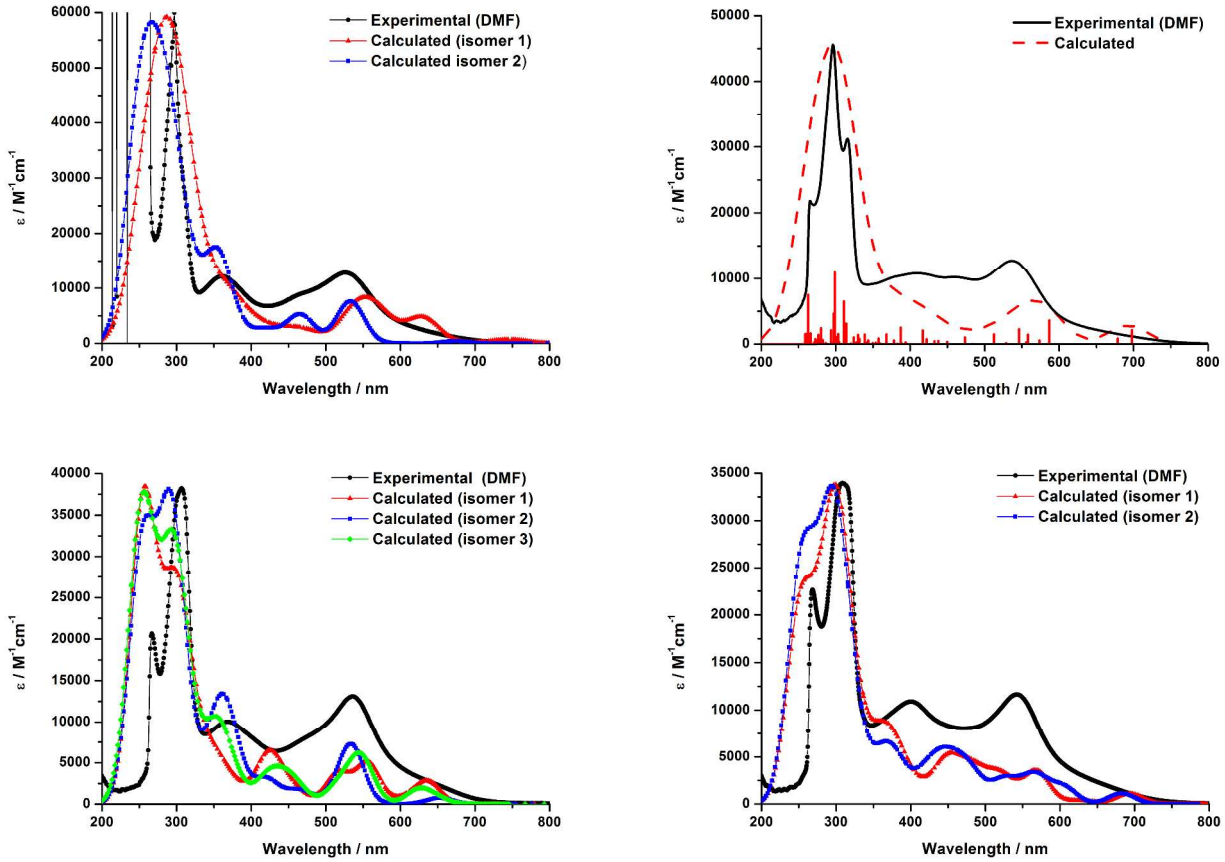

Fig. 3 Experimental and calculated absorption spectra of **1** (top left), **2** (top right), **3** (bottom left) and **4** (bottom right). See ESI† for isomer assignment.

Solar Measurements

Cells were prepared using screen printed TiO_2 with a thickness of 10 μm and an additional 5 μm scattering layer. The solvent used to dissolve the dye was altered between EtOH/DMSO (4:1, 0.3 mM, 24 h soaking time) or DMF (9 mM, 30 mins soaking time)[21] and we found higher efficiency for cells that use EtOH/DMSO, perhaps as a result of longer adsorption time.[22] Tetrabutylammonium deoxycholate ([TBA][DOC]), was used to deprotonate the acid group to help improve solubility and also to co-adsorb DOC to the TiO_2. Table S10 (ESI†) shows the results obtained.

The cells were optimised by changing the concentration of LiI in the electrolyte from 0.1-0.4 M. Increasing LiI concentration typically leads to an increase in photocurrent along with a slight decrease in photovoltage; resulting in an increase in efficiency. Li^+ can enhance the driving force for charge injection and also increase the effective diffusion coefficient of electrons in the mesoporous network, therefore increasing J_{sc}.[23, 24, 25] The downward shift in conduction band edge of TiO_2 however, may also result in a reduced V_{oc} and fill factor.[26] Across the series of dyes the IPCE data correlate very well with the absorption data, the measured J_{SC} values, and the increase in photocurrent of the cells with increasing LiI concentration.

Dyes **1-3** show an increase in photocurrent as the LiI concentration is increased (Table 3), which results in an increase in efficiency. The highest efficiency achieved for **4** however, was with 0.2 M LiI electrolyte. This is due to a decrease in fill factor using 0.4 M LiI along with a minimal change in photocurrent which correlates with the minimal change in IPCE data.

The most significant observation is that the solar cells with **3** and **1** gave much poorer efficiency than those with **2** and **4**. As noted above, **1**, **3** and **4** contain isomers, so over interpretation of

these data should be avoided, however it is striking that only **2** and **4**, containing the 4,4'-(CO_2H)-bipy binding ligand to TiO_2, showed high photocurrents, whereas **1** and **3**, containing only the single-anchoring-site 4,4'-(CO_2H,Me)-bipy ligand showed much reduced photocurrents. Alongside this, we note that cells with **1** showed a dramatic increase in photocurrent in response to the changes in LiI concentration, perhaps suggesting poor charge injection through the single-anchoring-site ligand, despite the higher-energy excited state for this dye shown in the emission spectrum (Table 1).

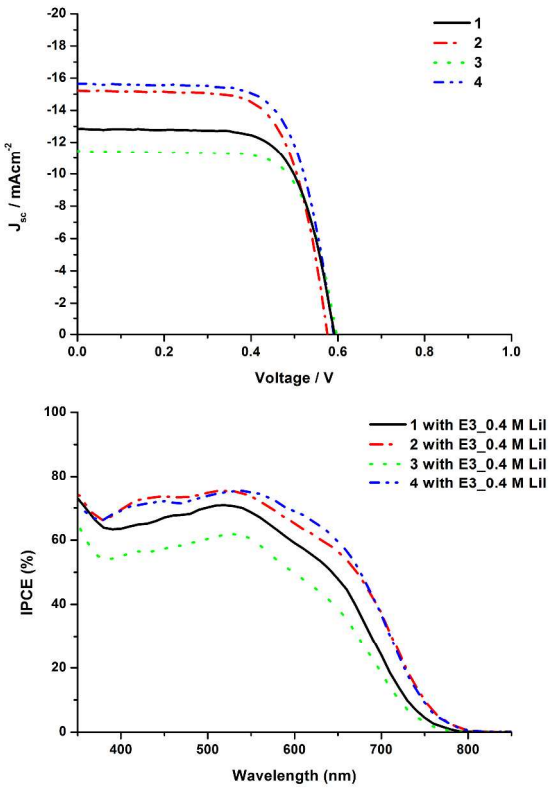

Fig. 4 JV (upper, best cells) and IPCE (lower, E3 electrolyte) comparison between dyes **1-4**.

Table 3 JV and IPCE data for complexes **1-4** and **N3**.

Dye	Electrolyte [a]	Voc / mV	Jsc / mAcm^{-2}	FF	η / %	Average η / %	$IPCE_{MAX}$ / % (λ / nm)
1	E1	600	9.96	0.71	4.22	4.15 ± 0.07	
	E2	580	10.64	0.70	4.34	-	
	E3	590	12.83	0.70	5.29	5.24 ± 0.05	71 (520)
2	E1	600	13.29	0.67	5.33	-	
	E2	600	14.57	0.68	5.95	-	
	E3	580	15.22	0.68	6.01	-	75 (510)
3	E1	590	10.33	0.72	4.40	4.34 ± 0.06	
	E2	590	10.95	0.72	4.64	4.26 ± 0.38	
	E3	600	11.44	0.71	4.89	4.68 ± 0.21	62 (530)
4	E1	590	14.90	0.70	6.16	5.96 ± 0.20	
	E2	590	15.65	0.69	6.37	6.29 ± 0.08	75 (540)
	E3	590	15.47	0.64	5.87	5.77 ± 0.10	
N3	Z960	680	17.37	0.71	8.33	-	86 (550)

[a] E1: 1M DMII, 0.1 M GuNCS, 0.1 M LiI, 0.03 M I_2, 0.5 M TBP, MeCN:VN (85:15)

E2: 1M DMII, 0.1 M GuNCS, 0.2 M LiI, 0.03 M I_2, 0.5 M TBP, MeCN:VN (85:15)

E3: 1M DMII, 0.1 M GuNCS, 0.4 M LiI, 0.03 M I_2, 0.5 M TBP, MeCN:VN (85:15)

Z960: 1M DMII, 0.1MGuNCS, 0.05 M LiI, 0.03 M I_2, 0.5 M TBP, MeCN:VN (85:15)

Dye Uptake and Binding

Optical Waveguide Spectroscopy (OWS) measurements can be used to understand the adsorption and desorption kinetics, dye diffusion and dye coverage within a DSSC.[11] OWS was used to measure dye uptake for all four dyes in DMF, monitoring the changes in refractive index (n) and molar extinction coefficient (k) in the solar cell as the dye entered the pores and adsorbed to the TiO_2 surface. In OWS measurements all the dye in the pores is measured, both free and surface attached, therefore at the end of an uptake measurement the film is washed for several hours with solvent to remove any loosely or non-bound dye.[11] The values obtained after the rinsing stage are a good estimate of the concentration of bound dye remaining in the TiO_2 pores. The

total refractive index change (Δn) is related to the amount of solvent displaced from the pores and replaced by dye molecules. In order to observe the waveguides, the film thickness was 1.5 μm instead of 10 μm used for JV measurements, thus the dye uptake rate will be quicker for the OWS analysis. Table 4 compares the total dye in the films for each of **1-4**. The concentration of dye is calculated as a function of total film volume.

Table 4 Total amount of dye in the films for complexes **1-4**, before and after the rinsing stage. The KOH desorption data were determined from UV-Vis measurements of similar films to those used for OWS and were used to check reasonable values were being obtained from the modelling.

Dye	Waveguide measurement after 140 minutes / molescm^{-3} of film volume	Waveguide measurement after complete dying and rinsing / molescm^{-3} of film volume	KOH Desorption experiment / molescm^{-3} of film volume
1	6.0×10^{-5}	9.3×10^{-5}	
2	1.2×10^{-4}	1.06×10^{-4}	$6.34 \times 10^{-5} \pm 4.5 \times 10^{-6}$
3	9.1×10^{-5}	1.3×10^{-4}	
4	1.1×10^{-4}	1.59×10^{-4}	$1.25 \times 10^{-4} \pm 6.8 \times 10^{-5}$

The change in concentration over time can be related to the change in the extinction coefficient, Δk (the concentration is calculated from Δk using the molar absorption coefficient for each dye at 633nm in DMF). Fig. 5 shows the kinetic plots for each dye during the first 140 minutes and Fig. 6 shows the full time course. Complexes **2** and **4** have dyed quickly, shown by steep initial kinetics, followed by a more gradual rise. For dye **2**, the concentration drops below the value at 140 minutes after rinsing, suggesting the majority of the dye attached at longer times was only weakly associated. Dye **4** produces the highest loading in comparison to the other three dyes. Binding of **4** fails to reach saturation and the rinsing stage was postponed until 40 hours to monitor the slow secondary increase. The kinetic plots for **1** and **3** indicate a slower initial adsorption rate. Both curves fail to reach saturation, and Δk continues to rise suggesting weakly-bound or aggregated dye is entering the pores. Interestingly, complex **3** has a higher concentration of dye remaining in the film in comparison to **2**, despite the slower initial uptake. For dye **1**, as well as slow uptake the lowest final concentration in the rinsed film is observed, indicating the weakest binding.

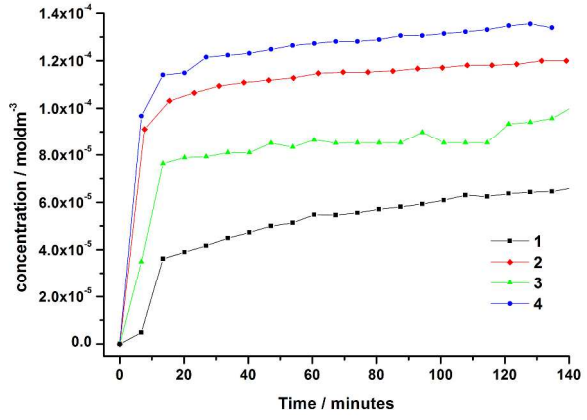

Fig.5 The initial change in concentration of dye inside the mesoporous TiO_2 film.

There is a noticeable trend whereby more CO_2H binding groups improves uptake of the dye and stronger adsorption to TiO_2. Dye **4**, with three acid groups, clearly has the most dye remaining in the pores after rinsing, which indicates the strongest binding to titania, followed by complexes **2** and **3**, then complex **1**. Complex **2** produces a very similar kinetic plot to **N719**[11] where the change in concentration begins to plateau at 4 hours. After rinsing the cell, the concentration of the dye quickly falls, suggesting the dye entering the film between 4-24 hours was only weakly bound.

The change in refractive index, Δn, was also monitored (Figure 7) and in the first 140 minutes (Fig. S13) largely corroborate the trends from Δk, although some slight differences are observed with respect to complex **3**. Previous studies have shown that Δn is less accurate than Δk at measuring concentration changes,[11] therefore the data have not been used to calculate a concentration change in the film. Again, the kinetic plot for **1** shows a very slow initial rise in Δn which indicates a poor dye uptake rate.

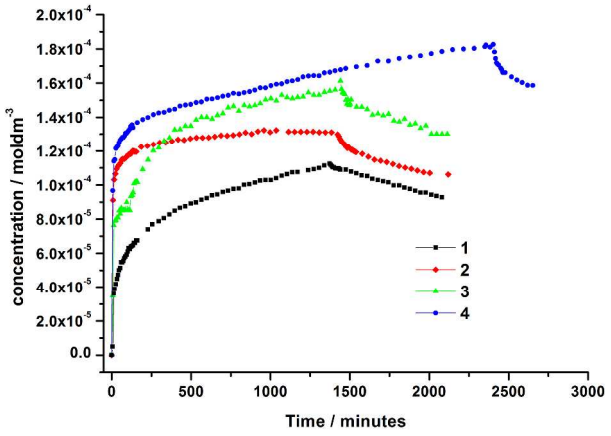

Fig.6 Change in concentration of complexes **1-4** within the mesoporous TiO_2 film during the dye uptake process. Illustrates the adsorption and desorption kinetics.

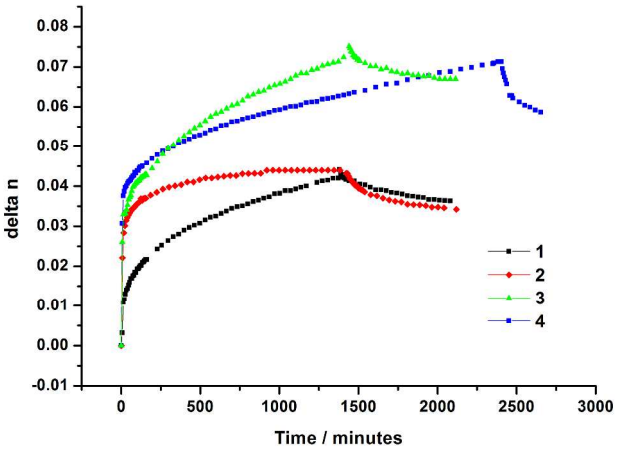

Fig.7 Overall changes in refractive index of complexes **1-4**.

Consideration of both Figures 6 and 7 compares the increase in

concentration of the dye in the film with the increase of refractive index of the film. Notably, over the whole timecourse, the Δn kinetic plot differs from the Δk plot. In particular, **3** now shows high dye loading. The increase in refractive index is due to the total number of dye molecules that displace solvent molecules in the pores and is therefore a measure of the total aggregated and non-aggregated dye in the film. In contrast, the extinction coefficient k does not increase linearly at high dye concentrations when aggregation occurs, as a result k can underestimate the dye in the film when significant aggregation takes place. This suggests that **3** shows considerable aggregation and the actual dye concentration should be higher than suggested by Δk. For **3**, dye aggregation may be increased due to the inclusion of an isomer with two acid groups *trans* to each other, such that one must remain unbound to the TiO_2. Thus, much of the higher binding of **3** over **2** may be attributed to aggregation, which is undesirable as it can quench the excited state resulting in lower injection yields.[27] This may partly explain the JV measurements where complex **3** gave a lower efficiency than **2**, despite similarly having two binding groups.

Figures 8 and S14 illustrate desorption rates during the rinsing stage to remove any weakly bound or unbound dye. Desorption kinetics are similar for dyes **2**-**4**, although slower for dye **1**. Although dye **1**, shows the lowest overall binding, there may also be less loosely-attached dye that can be easily rinsed away.

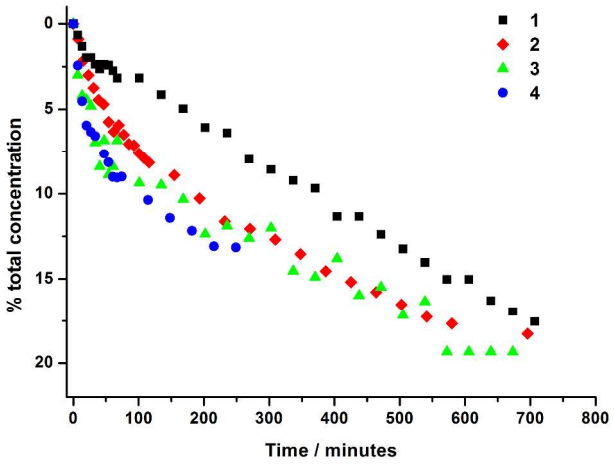

Fig.8 The total percentage of dye removed from the film during the rinsing stage.

Stability

Cells were prepared as described in the Experimental and stored under ambient conditions for one week prior to the thermal ageing process, to ensure the cells achieved a stable power output. The cells were then stored at 85 °C for 500 hours and JV measurements were recorded at time intervals of 0, 16, 176, 336 and 496 hours. Devices remained in the ageing chamber between measurements and were allowed to cool to room temperature before the JV data were collected. Fig. 9 illustrates the average change in the photovoltaic parameters of a subset of cells (four) from each group during the thermal storage. The JV parameters were collected at low light intensities (0.66 Wm^{-2}) relevant to indoor applications.

The general performance of these larger-area cells under low-light conditions matched the trends seen in the earlier JV-data, with **2** and **4** outperforming **1** and **3**. The change in V_{oc} showed an initial decrease and then plateaued after 16 hours with the exception of **1**, which showed a large drop of 122 mV over the course of 500 hours at 85 °C. The short-circuit current dropped steadily in a similar manner for **1**-**4** and unexpectedly showed a larger drop for the comparison N719 cells, although they always remained higher overall. The similar relative change in J_{SC} across all four dyes suggests loss of dye may be comparable in each case. In contrast however, the fill factor for the N719 and **2**-**4** cells did not significantly change during the thermal ageing process, whereas **1** showed a dramatic decrease (15 % loss) between 176-500 hours, matching the drop in V_{oc} over the same period. This could be attributed to a decrease in shunt resistance, which is more probable under low light conditions.

Overall **1**-**4** all maintained functioning cells after 500 hours at 85 °C, however dye **1**, with a single acid anchoring group, was most sensitive to degradation leading to a drop in performance parameters. Although desorption of **1** may not have been faster than for the other dyes, the lower starting quantity of **1** on the TiO_2 may contribute to a larger effect on V_{oc} via recombination as the amount of bound dye is reduced.

Conclusions

A series of four Ru(II) dyes with varying number of binding groups (CO_2H) has been synthesised, characterised and compared in dye-sensitised solar cells.

Increasing the number of electron-withdrawing groups (CO_2H) results in only a slight red-shift of the first absorption band in the visible region. Complexes **2** and **4** both emit at lower energy (725 nm) than **1** and **3**, likely due to the lower energy π-orbital on 4,4'-$(CO_2H)_2$-bipy that they both contain. In general however, the dyes have comparable electrochemical and photophysical properties to one another within the correct range for a working DSSC and can thus act as models to investigate binding and performance relating to the number of CO_2H groups.

The overall solar cell efficiency increased according to the number of CO_2H groups present; dye **4** consisting of three acid groups giving the best efficiency of 6.37%. Significantly however, the position of the acid groups was also seen to be crucial with **2** showing much higher J_{SC} than **3**. Notably, both dyes containing the 4,4'-$(CO_2H)_2$-bipy ligand (**2** and **4**) showed much higher J_{SC}. Altering the concentration of lithium iodide in the electrolyte caused an increase in photocurrent, resulting in an increase in overall efficiency and this was greatest for **1**, suggesting poor charge injection for this dye with one anchoring group.

The adsorption and desorption kinetics of each dye upon contact with TiO_2 was studied using OWS. Generally, increasing the number of binding groups resulted in stronger adsorption to TiO_2, faster dye uptake and greater dye coverage after rinsing. Complexes **2** and **4** showed the most rapid uptake, with the optimum adsorption time to be the first 5 hours. Dye **4** had the highest concentration of dye remaining in the cell after rinsing due to stronger binding to TiO_2. Similarly, a recent study on distinctive Ru(II) tridentate dyes also showed similar increase in both solution absorptivity and DSSC efficiencies according to the numbers of CO_2H group on the anchor.[28]

Solar cells were analysed via thermal ageing at 85 °C over 500 hours. The results showed that **2-4** were relatively stable, following similar trends as **N719**. Solar cells with dye **1** however showed a considerable decrease in V_{oc} and fill factor after 176 hours exposure, likely due to a decrease in shunt resistance.

The work reported here allows insight into dye design with respect to the number of carboxylic acid anchoring groups. The efficiency, rapid dye uptake, strong dye binding and thermal stability of the cell were all seen to be significantly poorer for dye **1** with a single acid group. This may have particular relevance to the field of organic dye design where the vast majority of novel dyes contain only one anchoring centre, albeit commonly cyanoacetic acid, rather than a simple carboxylic acid. Inclusion of two acid groups gave stronger binding than for **1**, however benefits to efficiency were only observed when these were attached to the same bipy ligand as in dye **2**. Addition of a third acid group gave advantages in dye attachment to TiO_2, however these translated into only modest improvements in cell efficiency and negligible differences to heat stability.

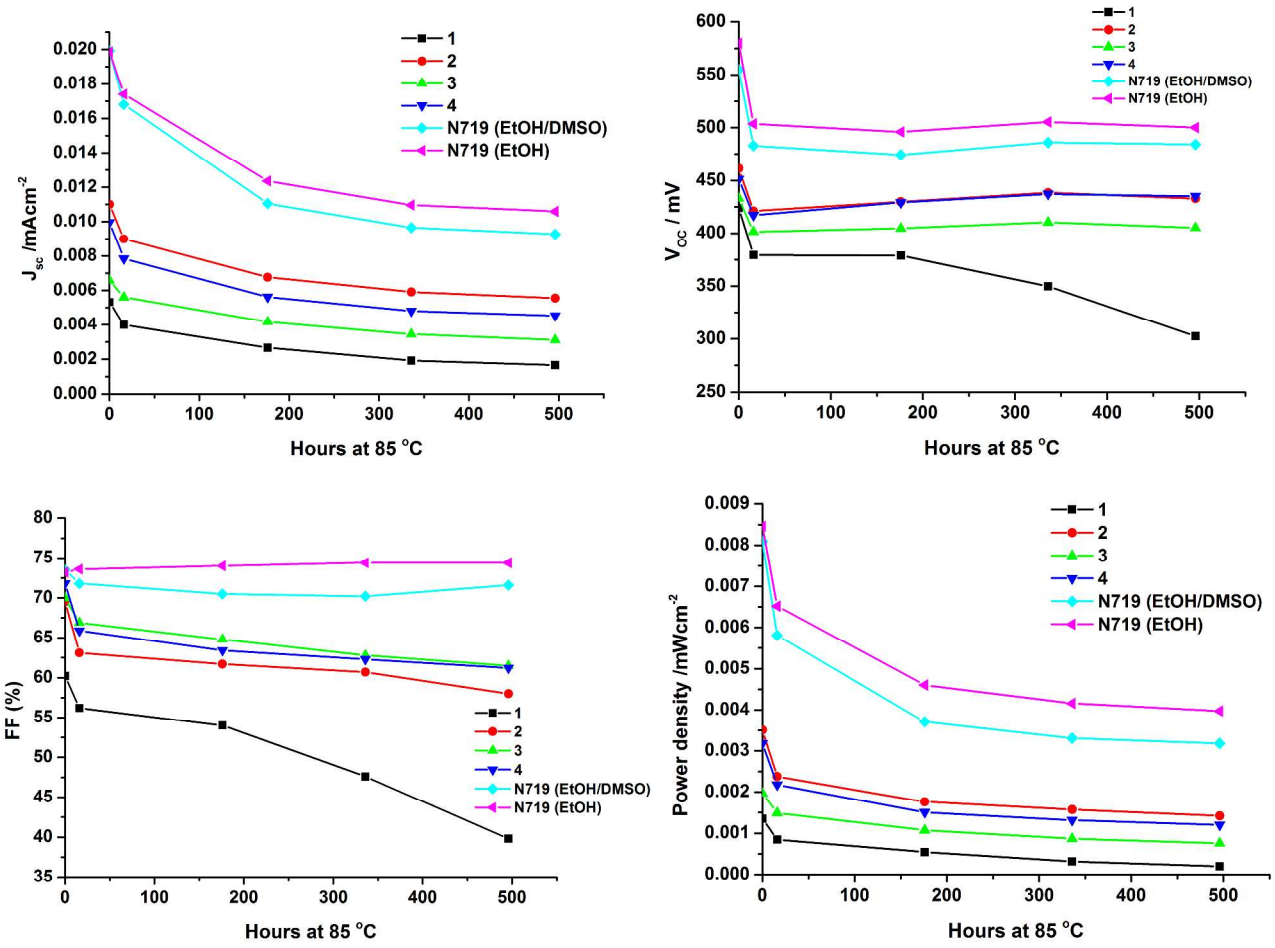

Fig.9 An average change in JV parameters for a set of four cells from each group (**1-4** and **N719** (EtOH/DMSO 4:1) and **N719** (EtOH)) during storage at 85 °C over a period of 500 hours. The measurements were conducted at 0.66 Wm^{-2}.

Experimental

The $[Ru(p\text{-cymene})Cl_2]_2$ precursor, 4,4'-dicarboxy-2,2'-bipyridine, [29] and 4-methyl-4'-carboxy-2,2'-bipyridine[30] were synthesised following literature procedures. 4,4'-dimethyl-2,2'-bipyridine was obtained from Sigma Aldrich and used as received.

All UV/Vis spectra were recorded using a JASCO V-670 series spectrophotometer and the data collected using Spectra Manager™ II software. Emission spectra for each ligand and complex were recorded at room temperature and 77 K in DMF, using a Fluoromax2 fluorimeter controlled by the ISAMain software. Electrochemical studies were recorded using the General Purpose Electrochemical System (GPES) software that was connected to an Autolab system containing a PGSTAT 30. The technique used a three-electrode system, with a Pt disk working electrode, a Pt rod counter electrode, and an Ag/AgCl reference electrode. The data are reported relative to NHE by adding +0.544 V to the potential observed versus an internal ferrocene/ferrocenium standard.[31] The supporting electrolyte was 0.1 M tetrabutylammonium tetrafluoroborate in DMF.

Theoretical calculations were performed using the Becke three parameters hybrid exchange and Perdew-Wang 1991 correlation functional (B3PW91).[32, 33] The Hay-Wadt VDZ (n+1) ECP [34-36] basis set was used to describe the ruthenium atom and all other atoms were described using the basis set 6-31 G*.[37] The initial

geometry was computed using Avogadro software.[38] Frequency calculations were measured on the optimised geometry to ensure that minimum energy was achieved. Time-dependent density functional theory (TD-DFT) calculations were used to compare the experimental and theoretical electronic transitions through absorption spectroscopy. Seventy singlet-singlet transitions were calculated using the optimised geometry surrounded by a DMF polarisable continuum model.

Cell fabrication: Fluorine-doped Tin Oxide (FTO) coated glass (3.2 mm thick, 9 Ω sheet resistance, Pilkington) was washed with detergent, water, acetone, and finally with ethanol. The glass was UV-ozone treated for 15 minutes (PSD series UV-ozone cleaning, Novascan Technologies, Inc.). The cleaned glass was treated with a dilute solution of $TiCl_4$ (40 mM, 75 ^oC for 30 mins), and rinsed with water, followed by ethanol. The mesoporous TiO_2 layer (20 nm particle size) was screen printed onto FTO glass. The layer was levelled and the glass was placed in an oven at 125 ^oC (5 minutes with the lid on and then 2 minutes without the lid). The glass was taken out of the oven and the process was repeated until a desired thickness was achieved (checked using a profilometer). A 5 μm light-scattering layer of anatase particles (400 nm, PST-400, JGC Catalysts and Chemicals, Japan) was screen printed on top of the previous TiO_2 layers. The TiO_2 electrodes (active area = 4x4 mm^2) were heated up to 500 °C for 30 min, cooled down to room temperature, treated with a dilute solution of $TiCl_4$ (40 mM, 75 ^oC for 30 mins) and sintered at 500 °C for 30 min. The electrodes were allowed to cool and were broken up into the desired size (15x15 mm^2). Hot electrodes (80-100 ^oC) were immersed into a dye bath solution for 30 minutes or 24 hours depending on the concentration and solvent used. In this work the dye bath solutions were either 0.3 mM ethanol:DMSO (4:1) (24 hours) or 9 mM DMF (30 minutes). The electrodes were removed and washed with ethanol, to remove any unbound dye. Meanwhile, counter electrodes were prepared by drilling two holes into pre-cut FTO glass (15x15 mm^2) and washed with detergent, water, acetone, and finally with ethanol. 10 μL of H_2PtCl_6 solution (5 mM) in isopropyl alcohol was dropped onto the FTO side and heated up to 400 ^oC for 15 minutes. The solar cells were assembled by sandwiching the two electrodes together using a sealant (Surlyn, 25 μm), without covering the active layer and ensuring the mask was overhanging to prevent short-circuit. The electrodes were heated up to 130 ^OC, applying even pressure to ensure the Surlyn melted evenly. Electrolyte was injected through the hole and the hole was sealed by Surlyn (60 μm) and a cover glass. The solar cell efficiency was collected using a simulator equipped with an AM 1.5G filter and a Keithley source meter with a four-wire setup. A mask was attached to the solar cell to absorb any scattered light.[39, 40]

For thermal stability measurements, working electrodes with an active area of 1 cm^2 were prepared by screen printing TiO_2 paste onto clean FTO glass substrates, followed by sintering. Solutions of dyes **1**, **2**, **3**, **4**, and N719 were prepared in 4:1 EtOH:DMSO, with an additional solution of N719 prepared in absolute EtOH. All solutions were 0.3 mM. Electrodes were sensitised by immersion in one of the above dye solutions for 18 hours. Sensitised working electrodes were rinsed and dried, followed by assembly with platinised counter electrodes, also on FTO glass, achieved by thermal compression of a 50 μm Bynel thermoplastic gasket between the electrodes. An electrolyte composed of iodine, 1-methyl-3-propyl imidazolium iodide (PMII), guanidinium thiocyanate (GuSCN), and N-methylbenzimidazole (NMB) in 3-methoxypropionitrile (MPN) was introduced into the cell through a pre-drilled hole, which was then sealed to complete the cell fabrication. Four cells were prepared for each dye. The relative humidity for the stability tests was 85%.

Optical waveguide spectroscopy (OWS) is described in detail in references 11 and 41. Briefly OWS was measured in the Kretschmann attenuated total internal reflection configuration on a home-built set-up. Laser (Uniphase, HeNe λ = 632.8 nm) light was passed through a chopper and two polarizers before being incident on one face of a LaSFN9 prism (Schott Glass). The chopper modulated the light at 1130 Hz and provided a reference signal for the lock-in amplifier (EG&G Instruments, 7265 DSP). The first polarizer was used to adjust the intensity of the incident light and the second one to ensure that only light with the desired polarization (i.e. TE or TM) reached the sample. The film of interest was formed on top of a ~50 nm gold film deposited on a LaSFN9 glass slide (Schott Glass) that was index-matched to the refractive index of the LaSFN9 prism by a thin layer of index matching fluid (Cargille Laboratories Inc., n = 1.700 ± 0.0002). The sample and the prism were mounted on top of a computer operated goniometer (Huber Two Circle Goniometer 410), which was used to control the precise angle of incidence of the light. The reflected light beam was focused through a collecting lens onto a silicon photodiode and the current measured using an integrated current amplifier (home built). A computer program (Wasplas, ResTek Gmbh) was used to measure the magnitude of reflected light reaching the photodiode as a function of the incident angle controlled by the goniometer. The OWS curves were fit using an iterative fitting program based on the Fresnel equations (Winspall, ResTek Gmbh). OWS was operated in reflection mode, in which the waveguide was illuminated from behind, through the gold layer, while the reflected intensity was measured as a function of the angle of incidence θ. This configuration was chosen as the guided light in the film is strongly attenuated over a short distance (in the μm-range) and therefore most accurately measured by the loss of reflected intensity. OWS spectra under p-polarised light were taken approximately every 10 minutes before and during uptake and each spectrum was fit separately to obtain the values of Δn and Δk reported here. The dye solutions were all 0.2 mmol dm^{-3} in DMF and were flowed slowly across the surface of the TiO_2 film during uptake. After several hours of uptake the films were rinsed by flowing DMF across the surface and the drop in the concentration of dye within the film monitored. The extinction coefficient k is directly related to the absorption cross-section for the dye which was obtained from UV-Vis measurements, calibration curves were prepared using several different concentration dye solutions illuminated at 633nm. The values for the absorption cross-section were 1.31591E-17, 1.36628E-17, 1.26701E-17, 1.33085E-17 for dyes **1**-**4** respectively and could be used to relate the change in k to the change in dye concentration within the film. Dye desorption data was collected for two of the

dyes (table 4) to ensure similar final dye concentrations in the films were being obtained for OWS and desorption measurements. This check is performed to ensure the model being used to fit the OWS data is valid. The desorption measurements were taken for titania films that were prepared in an identical manner to the films used for OWS and the average of three measurements was taken. As the measurements are not of the same film it is not expected that the desorption results will be identical to those obtained by OWS, however the results are within experimental error of each other.

Synthesis of Ru(dmbpy)(mcbpy)(NCS)$_2$ [1].

[Ru(*p*-cymene)Cl$_2$]$_2$ (180 mg, 0.29 mmol) was dissolved in DMF (60 mL) and heated to 60 ^{o}C, under a nitrogen atmosphere and kept in reduced light. Dmbpy (108 mg, 0.59 mmol) was added and the mixture was heated for 4 hours. Mcbpy (125 mg, 0.59 mmol) was added and the reaction was refluxed for 4 hours at 155 ^{o}C. Ammonium thiocyanate (1818 mg, 15.5 mol) was transferred to the flask and the mixture was refluxed for a further 4 hours. The sample was cooled down and the solvent was removed *in vacuo*. Water (about 40 mL) was transferred to the flask and the mixture was stirred overnight to remove excess ammonium thiocyanate. The red solid was filtered and washed with water and then ether. The crude material was purified on Sephadex LH-20 using DMF as the eluent, and solvent was removed from the main red band. The pure red product was washed with copious amounts of water and ether and dried under high vacuum. Yield: 86.5 mg, 24.0 %. ^{1}H NMR (DMSO, 500 MHz)/ppm: δ 9.44 (d, 1H, H-bpy)^1, 9.08 (d, 1H, H-bpy)^1, 9.07 (d, 1H, H-bpy)^2, 9.03 (d, 1H, H-bpy)^2, 8.97 (s, 1H, H-bpy)^1, 8.82 (d, 1H, H-bpy)^2, 8.82 (d, 1H, H-bpy)^2, 8.69 (s, 1H, H-bpy)^1, 8.62 (s, 1H, H-bpy)^1, 8.61 (s, 1H, H-bpy)^2, 8.47 (s, 1H, H-bpy)^1, 8.47 (s, 1H, H-bpy)^2, 8.24 (d, 1H, H-bpy)^1, 7.80 (s, 1H, H-bpy)^2, 7.79 (s, 1H, H-bpy)^2, 7.78 (d, 1H, H-bpy)^1, 7.76 (d, 1H, H-bpy)^2, 7.57 (dd, 1H, H-bpy)^2, 7.38 (d, 1H, H-bpy)^1, 7.35 (d, 1H, H-bpy)^1, 7.30 (d, 1H, H-bpy)^2, 7.13 (d, 1H, H-bpy)^1, 7.09 (d, 1H, H-bpy)^2, 7.05 (d, 1H, H-bpy)^1, 2.67 (s, 3H, CH$_3$)^2, 2.66 (s, 3H, CH$_3$)^1, 2.65 (s, 3H, CH$_3$)^2, 2.42 (s, 3H, CH$_3$)^1, 2.39 (s, 3H, CH$_3$)^2, 2.39 (s, 3H, CH$_3$)^1 where ^{1} represents isomer 1 and ^{2} represents isomer 2. +ESI/MS: 616.02 [M+H]$^+$. Anal. Calc. For $C_{26}H_{22}N_6O_2RuS_2$: C 50.72 H 3.60 N 13.65. Found: C 50.57 H 3.41 N 13.49.

Synthesis of Ru(dmbpy)(dcbpy)(NCS)$_2$ [2].

Followed the same procedure as [**1**] but added in dcbpy (144 mg, 0.59 mmol) instead. Yield: 111.3 mg, 29.4 %. ^{1}H NMR (DMSO, 500 MHz)/ppm: δ 9.45 (d, 1H, J = 5.8 Hz, H-bpy), 9.09 (s, 1H, H-bpy), 9.05(d, 1H, J = 5.7 Hz, H-bpy), 8.94 (s, 1H, H-bpy), 8.66 (s, 1H, H-bpy), 8.50 (s, 1H, H-bpy), 8.31 (dd, 1H, J = 1.7 Hz, 5.8 Hz, H-bpy), 7.83 (d, 1H, J = 5.8 Hz, H-bpy), 7.83 (d, 1H, J = 5.8 Hz, H-bpy), 7.63 (dd, 1H, J = 1.7 Hz, 6 Hz, H-bpy), 7.31 (d, 1H, J = 5.8 Hz, H-bpy), 7.06 (d, 1H, J = 5.8 Hz, H-bpy), 2.67 (s, 3H, CH$_3$), 2.40 (s, 3H, CH$_3$). +ESI/MS: 668.90 [M+Na]$^+$. –ESI/MS: 644.78 [M-H]$^-$. Anal. Calc. For $C_{26}H_{20}N_6O_4RuS_2$: C 48.36 H 3.12 N 13.02. Found: C 48.42 H 3.23 N 13.09.

Synthesis of Ru(mcbpy)$_2$(NCS)$_2$ [3].

[Ru(*p*-cymene)Cl$_2$]$_2$ (180 mg, 0.29 mmol) was dissolved in DMF (60 mL) and heated to 60 ^{o}C, under a nitrogen atmosphere and kept in reduced light. Mcbpy (250 mg, 1.18 mmol) was added and the reaction mixture was refluxed at 155 ^{o}C for 8 h. Ammonium thiocyanate (1818 mg, 15.5 mol) was transferred to the flask and the mixture was refluxed for a further 4 hours. The sample was cooled down and the solvent was removed *in vacuo*. Water (about 40 mL) was transferred to the flask and the mixture was stirred overnight to remove excess ammonium thiocyanate. The red solid was filtered and washed with water and then ether. The crude material was purified on Sephadex LH-20 using DMF as the eluent. The pure red product (after removing solvent) was washed with copious amounts of water and ether and dried under high vacuum. Yield: 97.4 mg, 25.7 %. ^{1}H NMR (DMSO, 500 MHz)/ppm: δ 9.45 (d, 1H, J = 5.67 Hz, H-bpy)^2, 9.41 (d, 1H, J = 5.68 Hz, H-bpy)^1, 9.08 (d, 2H, J = 5.68 Hz, H-bpy)$^{1, 3}$, 9.03 (d, 1H, J = 5.68 Hz, H-bpy)^2, 9.01 (s, 3H, H-bpy)$^{1, 2, 3}$, 8.87 (s, 3H, H-bpy)$^{1, 2, 3}$, 8.85 (s, 3H, H-bpy)$^{1, 2, 3}$, 8.74 (s, 1H, H-bpy)^1, 8.72 (s, 2H, H-bpy)$^{2, 3}$, 8.29 (d, 1H, J = 4.57 Hz, H-bpy)^2, 8.28 (d, 1H, J = 4.89 Hz, H-bpy)^1, 7.84 (d, 3H, J = 6.31 Hz, H-bpy)$^{1, 3}$, 7.83 (d, 2H, J = 6.15 Hz, H-bpy)$^{2, 3}$, 7.78 (d, 2H, J = 5.83 Hz, H-bpy)$^{2, 3}$, 7.73 (d, 2H, J = 5.83 Hz, H-bpy)$^{1, 3}$, 7.59 (d, 2H, J = 5.36 Hz, H-bpy)$^{1, 3}$, 7.53 (d, 2H, J = 5.83 Hz, H-bpy)$^{2, 3}$, 7.41 (d, 1H, J = 5.83 Hz, H-bpy)^2, 7.35 (d, 1H, J = 5.68 Hz, H-bpy)^1, 7.14 (d, 1H, J = 5.52 Hz, H-bpy)^1, 7.09 (d, 1H, J = 5.36 Hz, H-bpy)^2, 2.68 (s, 6H, CH$_3$)$^{1, 3}$, 2.67 (s, 3H, CH$_3$)^2, 2.42 (s, 9H, CH$_3$)$^{1, 2, 3}$ where ^{1} represents isomer 1, ^{2} represents isomer 2, and ^{3} represents isomer 3. –ESI/MS: 645.02 [M-H]$^-$. Anal. Calc. For $C_{26}H_{20}N_6O_4RuS_2$: C 48.36 H 3.12 N 13.02. Found: C 48.21 H 3.25 N 12.92.

Synthesis of Ru(mcbpy)(dcbpy)(NCS)$_2$ [4].

Followed the same procedure as [**1**] but added in mcbpy (125 mg, 0.59 mmol) instead of dmbpy and dcbpy (144 mg, 0.59 mmol) instead of mcbpy. Yield: 181.5 mg, 45.7 %. ^{1}H NMR (DMSO, 500 MHz)/ppm: δ 9.45 (d, 1H, J = 6.1 Hz, H-bpy)^2, 9.41 (d, 2H, J = 5.6 Hz, H-bpy)^{1,2}, 9.10 (s, 2H, H-bpy)^{1,2}, 9.05 (d, 1H, J = 5.6 Hz, H-bpy)^1, 9.03 (s, 1H< H-bpy)^2, 8.94 (s, 1H, H-bpy)^1, 8.94 (s, 1H, H-bpy)^2, 8.88 (s, 1H, H-bpy)^1, 8.86 (s, 1H, H-bpy)^1, 8.74 (s, 1H, H-bpy)^2, 8.33 (d, 1H, H-bpy)^2, 8.31 (d, 1H, H-bpy)^1, 8.31 (d, 1H, H-bpy)^2, 7.86 (d, 1H, J = 5.9 Hz, H-bpy)^1, 7.82 (d, 1H, J = 6.4 Hz, H-bpy)^2, 7.78 (d, 1H, J = 5.9 Hz, H-bpy)^1, 7.71 (d, 1H, J = 6.1 Hz, H-bpy)^1, 7.63 (dd, 1H, J = 1.1, 5.9 Hz, H-bpy)^1, 7.58 (dd, 1H, J = 1.3, 5.9 Hz, H-bpy)^2, 7.55 (dd, 1H, J = 1.3, 5.9 Hz, H-bpy)^1, 7.37 (d, 1H, J = 6.1 Hz, H-bpy)^2, 7.11 (d, 1H, J = 5.9 Hz, H-bpy)^2, 2.69 (s, 3H, CH$_3$)^1, 2.42 (s, 3H, CH$_3$)^2 where ^{1} represents isomer 1 and ^{2} represents isomer 2. –ESI/MS: 674.90 [M-H]$^-$. Anal. Calc. For $C_{26}H_{18}N_6O_6RuS_2$: C 46.22 H 2.69 N 12.44. Found: C 46.12 H 2.79 N 12.36.

Acknowledgements

We thank EPSRC (EP/G031088 and EP/K004468) for financial support. This work has made use of the resources provided by the EaStChem Research Computing Facility (http://www.eastchem.ac.uk/rcf). This facility is partially

supported by the eDIKT initiative (http://www.edikt.org).

Notes and references

[a] *School of Chemistry and EaStCHEM, University of Edinburgh, King's Buildings, Edinburgh, UK.*
Fax: +44 131 650 4743; Tel: +44 131 650 4755; E-mail: neil.robertson@ed.ac.uk
[b] *Department of Chemistry, University of Bath, Bath, UK.*
[c] *SolarPrint Ltd, Sandyford, Dublin, Ireland*
[d] *Department of Chemistry, National Tsing Hua University, HsinChu, Taiwan, R.O.C*

†Electronic Supplementary Information (ESI) available: Figure S1, Table S1: Isomers of **1-4**; Figure S2: ^{1}H NMR of **3**; Figure S3: Excitation and emission spectra of **1-4**; Figure S4: Electrochemistry of **3**; Figure S5 Photocurrent-voltage curve for **1** with varying TiO_2 film thickness; Figure S6: JV and IPCE data for **N3**; Figure S7: IPCE graph of **1** with Z960 electrolyte. Changes to the solvent system and film thickness; Figure S8: JV and IPCE graphs of **1**; Figure S9: JV and IPCE graphs of **2**; Figure S10: JV and IPCE graphs of **3**; Figure S11: JV and IPCE graphs of **4**; Figure S12: UV-Vis spectra of surface bound dye; Figure S13: Change in refractive index within the film for the first 140 minutes; Figure S14: Changes in concentration of dye in the film during the initial rinsing stage Table S2: Percentage contributions from component parts of **1** to selected molecular orbitals; Table S3: Percentage contributions from component parts of **2** to selected molecular orbitals ; Table S4: Percentage contributions from component parts of **3** to selected molecular orbitals; Table S5: Percentage contributions from component parts of **4** to selected molecular orbitals; Table S6: TD-DFT calculated visible absorption wavelengths of **1**; Table S7: TD-DFT calculated visible absorption wavelengths of **2**; Table S8: TD-DFT calculated visible absorption wavelengths of **3**; Table S9: TD-DFT calculated visible absorption wavelengths of **4**; Table S10: JV data for **N3** with varying film thickness using Z960 electolyte. Table S11 JV data for 1 with varying TiO_2 thickness and solvent system; For ESI see DOI: 10.1039/b000000x/
.

1 A. Hagfeldt, G. Boschloo, L. Sun, L. Kloo, H. Pettersson, *Chem. Rev.* 2010**, 110**, 6595
2 B. E. Hardin, H. J. Snaith, M. D. McGehee, *Nature Photonics*, 2012, **6**, 162
3 S. Zhang, X. Yang, Y. Numata, L. Han, *Energy Environ. Sci*., 2013, **6**, 1443
4 C.A. Bignozzi, R. Argazzi, R. Boaretto, E. Busatto, S. Carli, F. Ronconi, S. Caramori, *Coord. Chem. Rev*. 2013, **257**, 1472
5 K. C. D. Robson, P. G. Bomben, C. P. Berlinguette, *Dalton Trans*., 2012, **41**, 7814
6 B. Bozic-Weber, E. C. Constable, C. E. Housecroft, *Coord. Chem. Rev*. 2013, **257**, 3089
7 J. N. Clifford, M. Planells, E. Palomares, *J. Mater. Chem*., 2012, **22**, 24195
8 M. V. Martinez-Diaz, G. de la Torrea, T. Torres, *Chem. Commun.,* 2010, **46**, 7090
9 J. N. Clifford, A. Forneli, H. Chen, T. Torres, S. Tan, E. Palomares, *J. Mater. Chem*., 2011, **21**, 1693
10 W. Macyk, K. Szaciłowski, G. Stochel, M. Buchalska, J, Kuncewicz, P. Łabuz, *Coord. Chem. Rev.*, 2010, **254**, 2687
11 A. Peic, D. Staff, T. Risbridger, B. Menges, L. M. Peter, A. B. Walker, P. J. Cameron, *J. Phys. Chem. C*, 2011, **115**, 613
12 A. Listorti, B. O'Regan, J. R. Durrant, *Chem. Mater.,* 2011, **23**, 3381
13 F. De Angelis, S. Fantacci, A. Selloni, M. K. Nazeeruddin, M. Gra□tzel, *J. Phys. Chem. C*, 2010, **114**, 6054
14 X. Yang, S. Zhang, K. Zhang, J. Liu, C. Qin, H. Chen, A. Islam, L. Han, Energy Env. Sci., 2013, DOI:10.1039/C3EE42110D
15 P. Wang, S. M. Zakeeruddin, J. E. Moser, M. K. Nazeeruddin, T. Sekiguchi, M. Grätzel, *Nature Mater.,* 2003, **2**, 402
16 D. L. Pavia, G. M. Lampman, G. S. Kriz, J. R. Vyvyan, *Introduction to Spectroscopy*, 4th Edition, 2009, Brooks/Cole Cengago Learning Publishing.
17 Md. K. Nazeeruddin, A. Kay, I. Rodicio, R. Humphry-Baker, E. Müller, P. Liska, N. Vlachopoulos, M. Grätzel, *J. Am. Chem. Soc.*, 1993, **115**, 6382
18 A. Graczyk, F. A. Murphy, D. Nolan, V. Fernández-Moreira, N. J. Lundin, C. M. Fitchett, S. M. Draper, *Dalton Trans.*, 2012, **41**, 7746
19 G. Boschloo, E. A. Gibson, A. Hagfeldt, *J. Phys. Chem. Lett.,* 2011, **2**, 3016
20 K. L. McCall, J. R. Jennings, H. Wang, A. Morandeira, L. M. Peter, J. R. Durrant, L. J. Yellowlees, J. D. Woollins, N. Robertson, *J. Photochem, Photobiol. A,* 2009, **202**, 196
21 Md. K. Nazeeruddin, R. Splivallo, P. Liska, P. Comte, M. Grätzel, *Chem. Comm.*, 2003, 1456
22 W-C. Chang, C-H. Lee, W-C. Yu, C-M. Lin, *Nanoscale Res. Lett.*, 2012, **7**, 1
23 S. J. Smalley, M. R. Waterland, S. G. Telfer, *Inorg. Chem.*, 2009, **48**, 13
24 J. Wu, Z. Lan, S. Hao, P. Li, J. Lin, M. Huang, L. Fang, Y. Huang, *Pure and Applied Chem*., 2008, **80**, 2241
25 J. R. Jennings, Q. Wang, *J. Phys. Chem. C*, 2010, **114**, 1715
26 S-Y. Ku, S-Y. Lu, *Int. J. Electrochem. Sci*. 2011, **6**,5219
27 J. N. Clifford, E. Martínez-Ferrero, A. Viterisi, E. Palomares, *Chem. Soc. Rev*., 2011, **40**, 1635
28 K. Chen, Y.-H. Hong, Y. Chi, W.-H. Liu, B.-S. Chen and P.-T. Chou, *J. Mater. Chem.*, 2009, **19**, 5329
29 P. G. Hoertz, A. Staniszewski, A. Marton, G. T. Higgins, C. D. Incarvito, A. L. Rheingold, G. J.Meyer, *J. Am. Chem. Soc.*, 2006, **128**, 8234
30 W. S. Perry, S. J. A. Pope, C. Allain, B. J. Coe, A. M. Kenwright, S. Faulkner, *Dalton Trans.*, 2010, **39**, 10974
31 I. Noviandri, K. N. Brown, D. S. Fleming, P. T. Gulyas, P. A. Lay, A. F. Masters, L. Phillips, *J. Phys. Chem. B*, 1999, **103**, 6713
32 J. P. Perdew, J. A. Chevary, S. H. Vosko, K. A. Jackson, M. R. Pederson, D. J. Singh, C. Fiolhais, *Phys. Rev. B*, 1993, **48**, 4978
33 J. P. Perdew, K. Burke, Y. Wang, *Phys. Rev. B*, 1996, **54**, 16533
34 P. J. Hay, W. R. Wadt, *J. Chem. Phys.*, 1985, **82**, 270
35 W. R. Wadt, P. J. Hay, *J. Chem. Phys.*, 1985, **82**, 284
36 P. J. Hay, W. R. Wadt, *J. Chem. Phys.*, 1985, **82**, 299
37 M. M. Francl, W. J. Pietro, W. J. Hehre, J. S. Binkley, M. S. Gordon, D. J. Defrees, J. A. Pople, *J. Chem. Phys.,* 1982, **77**, 3654
38 Avogadro 1.1.0, http://sourceforge.net/projects/avogadro/
39 K. Kalyanasundaram, *Dye-Sensitized Solar Cells*, EPFL Press, CRC Press: Taylor and Francis Group, LLC, 2010.
40 C-W. Hsu, S-T. Ho, K-L. Wu, Y. Chi, S-H. Liu, P-T. Chou, *Energy and Environmental Sci*., 2012, **5**, 7549
41 P. J. Cameron, A. T. A. Jenkins, W. Knoll, F. Marken, E. V. Milsom, T. L. Williams, *J. Mater. Chem.* 2008, **18**, 4304